Characterization of Sonochemically Prepared Unsupported and Silica-Supported Nanostructured Pentavalent Molybdenum Oxide

N. Arul Dhas and A. Gedanken*

Department of Chemistry, Bar-Ilan University, Ramat-Gan 52900, Israel

Received: April 24, 1997; In Final Form: August 5, 1997[⊗]

We describe the preparation and characterization of unusual pentavalent molybdenum oxide stabilized by water molecules, $Mo_2O_5 \cdot 2H_2O$. Ultrasound irradiation of a slurry of molybdenum hexacarbonyl, $Mo(CO)_6$, in Decalin for 3 h under ambient air yields blue-colored $Mo_2O_5 \cdot 2H_2O$. Infrared (FT-IR) spectrum analysis of the resulting blue product reveals that the Mo ions possess molybdenyl bonds (Mo═O) and Mo−O character and also shows the presence of hydrogen-bonded, as well as coordinated, water molecules. The DSC profile of the blue oxide shows the presence of two endothermic peaks at around 100 °C and 140 °C, corresponding to the elimination of hydrogen-bonded and coordinated water molecules, respectively. The amount of water molecules was determined by thermogravimetric analysis (TGA). Characterization using powder X-ray diffraction (XRD) and transmission electron microscopy (TEM) with selected area electron diffraction (SAED) shows the amorphous nature of the blue product. The TEM picture shows that the blue oxide is composed of spongy platelet nanoparticles (∼20 nm). Heating the initial blue powder at 300 °C for 2 days under an oxygen, hydrogen, and nitrogen atmosphere yields X-ray crystalline MoO_3, MoO_2, and a mixture of MoO_3 and MoO_2, respectively. X-ray photoelectron spectroscopy (XPS), along with the potentiometric titration analysis of the blue oxide, confirms the formation of pentavalent molybdenum oxide. UV−visible absorption studies of the blue product demonstrate that the characteristic absorption of the Mo(V) (d^1-cation) oxide system and the Mo ions probably consists of two types of coordination symmetry (T_d and O_h). Electron spin resonance (ESR) experimental results revealed an unusual doublet pattern, which is ascribed to superhyperfine coupling of pentavalent molybdenum with a proton of coordinated water. The nanostructured amorphous pentavalent molybdenum oxide (blue oxide) thus formed has also been successfully deposited on Stober's silica microperes (250 nm) ultrasonically. The TEM images of silica-supported blue oxide reveal uniform distribution and strong adhering nature of the blue oxide. FT-IR spectroscopy illustrated the structural changes that occur when the amorphous SiO_2 is coated sonochemically with the blue oxide.

Introduction

Synthesis of unusual and nanometer-scale materials has been the focus of intense study in materials science and solid-state chemistry.[1] Owing to the diversity in the preparation of these materials, a broad spectrum of physical and chemical properties is possible. The growing interest in the chemistry of pentavalent oxides of molybdenum, so-called "blue oxides," stems from their attractive electrochromic properties, apart from their interesting electrochemical, spectroscopic characteristics.[2] It has been suggested that the coloration phenomena of this oxide may be useful for memory devices. Studies on pentavalent molybdenum species continue to be of interest in biology, largely because of their relevance to the active sites of molybdenum enzymes.[3]

The most stable oxides of molybdenum are MoO_2 and MoO_3, where the oxidation states of Mo are tetravalent and hexavalent, respectively. MoO_2 has a distorted rutile structure, whereas MoO_3 forms a unique layer structure composed of distorted [MoO_6] octahedra.[1b] Hydrated mixed molybdenum(V/VI) oxides, known as "blue oxides," have essentially the same layer structure as MoO_3. The water molecules reside between the layers, through hydrogen bonding, or are coordinated to the metal center.[4] Pentavalent molybdenum oxide (Mo_2O_5) is highly unstable. However, it has been shown that the insertion of hydrogen, alkali, and alkaline metals between the molybdenum oxide layers of stable MoO_3 allows for the stabilization of pentavalent molybdenum. These classes of technologically important compounds are called molybdenum bronzes.[1b] Recent work on molybdenum phosphates have shown that the pentavalent molybdenum can be stabilized in a phosphate matrix.[5] Formation of oxygen-deficient or vacancy-stabilized pentavalent molybdenum oxides has also been observed by the thermal[6] and electrochemical[7] reduction of Mo(VI) oxides. Anbanathan and co-workers[7b] have observed the formation of oxygen-deficient molybdenum oxide under electrochemical reduction of molybdenum trioxide. They suggest, from the IR and XRD results, that the resulting oxygen-deficient blue oxide corresponds to neither hydrogen bronzes nor any other known phases of molybdenum oxide.

Molybdenum oxides, for example, are of fundamental importance to the catalytic community, and supported molybdenum oxides have been used as an industrial catalyst for large scale productions of reactions such as hydrodesulfurization of petrol, coal liquefaction, hydrogenation, oxidation, polymerization, and metathesis of olefins.[8] It has been recognized that the participation of $(Mo{=}O)^{3+}$ oxide species in molybdenum oxide catalysts probably provides the active site for most of the catalytic reactions. The molybdenum oxide catalyst is frequently adsorbed on a high surface area support, usually silica, alumina, etc., by wet impregnation techniques. To have an optimum catalytic performance, certain "design criteria" must be fulfilled by the catalyst material.[9] They are (i) retention of the nanoscale dimension of the active phase, since, the smaller the size of the catalytic active species, the larger the fraction of the atoms exposed at surfaces, where they are accessible to reactant

* Corresponding author. E-mail: gedanken@ashur.cc.biu.ac.il. Fax: + 972-3-5351250.

⊗ Abstract published in *Advance ACS Abstracts,* October 15, 1997.

S1089-5647(97)01385-0 CCC: $14.00

molecules and available for catalysis; (ii) effective interaction between the active phase and the solid support; (iii) uniform distribution of the active phase on the surface of the support. It is generally accepted that the "weak" interaction occurring between MoO_3 and its underlying SiO_2 support accounts for a relatively fast reduction and poor dispersion of the active MoO_3 phase. This is a consequence of the acidic nature of the silica and the low density and reactivity of its hydroxyl population, which do not allow for an effective interaction with Mo oxides. Agglomeration and incipient sintering of the oxide phase during drying and calcination treatments have been observed in MoO_3/SiO_2 catalyst prepared by impregnation with aqueous solutions of molybdenum compounds.[8] Considerable effort has been paid, viz. ion-sputtering, vaporization, and grafting techniques,[10] to meet the "design criteria". Because molybdenum oxide interacts only weakly with silica, the effectiveness in producing samples with high dispersion or uniform structure has been limited. Therefore, synthesis of supported nanoscale catalyst materials still represents a synthetic challenge in the field of advanced catalysis, despite several new approaches.

Recently, sonochemical processing has been proven to be a useful technique to generate novel materials with desirable properties.[11] The chemical effects of ultrasound arise from acoustic cavitation: formation, growth, and implosive collapse of bubbles in liquid. The implosive collapse of the bubble generates localized hot spots through adiabatic compression or shock wave formation within the gas phase of the collapsing bubble. The conditions formed in these hot spots have been experimentally determined, with transient temperatures of ~5000 K, pressures of 1800 atm, and cooling rates in excess of 10^{10} K/s. These extreme conditions attained during bubble collapse have been exploited to decompose the metal−carbonyl bonds and generate metals,[11b,c] metal carbides,[11d] and metal oxides.[11e] Ultrasound irradiation of molybdenum hexacarbonyl under an argon atmosphere yielded molybdenum carbide.[11d] However, until now there has been no report on the bulk preparation and characterization of unusual, simple Mo_2O_5 blue oxide material. Herein, we report the characterization of an unusual pentavalent molybdenum oxide (henceforth referred as blue oxide) prepared by the ultrasound irradiation of $Mo(CO)_6$ in Decalin under air near room temperature. Characterization using various different techniques, such as infrared (FT-IR), themogravimetry (TG), differential scanning calorimetry (DSC), powder X-ray diffraction (XRD), X-ray photoelectron (XPS), UV−visible spectroscopy, and electron spin resonance (ESR) spectroscopy, confirmed the formation of water-stabilized pentavalent molybdenum oxide. Also, we report on the method for preparing desirable silica-supported blue oxide catalyst sonochemically.

2. Experimental Section

Materials. Dried and degassed Decalin (98%, Sigma) were used for the sonication. $Mo(CO)_6$ was purchased from Aldrich (purity 98%) and was not further purified. Ultrasonic irradiation was accomplished with a high-intensity ultrasonic probe[12] (Misonix, XL sonifier, 1 cm diameter Ti horn, 20 kHz, 100 W cm^{-2}). A round-bottom Pyrex glass vessel (total volume 110 mL, diameter 27 mm o.d) was used for the ultrasound irradiation, which was carried out under ambient air.

Sonochemical Synthesis. *A. Blue Oxide.* A slurry of molybdenum hexacarbonyl (2 g in 100 mL of Decalin) was sonicated with a high-intensity ultrasonic horn (direct immersion) at room temperature for 3 h, under ambient air. The temperature of the bulk (inside the sonication vessel) rose to 90 °C during sonication, as measured using an IC thermocouple. On irradiation, the colorless slurry turned blue and gradually became more intense with increased irradiation. The observed gradual increased intensity of the color indicates the formation process of a blue product as irradiation time progressed. The reaction was carried out for 3 h to make complete decomposition/oxidation of the molybdenum metal carbonyl in the reaction mixture; otherwise, the blue product would have been contaminated by the starting precursor. The resulting blue powder was recovered by centrifugation, was washed several times with dry pentane, and was dried in a vacuum. The blue powder obtained is soluble in water, acetonitrile, ethanol, and benzene.

B. Silica-Supported Blue Oxide. To obtain silica-supported blue oxide, 300 mg of activated Stober's silica was added in the reaction mixture (a slurry of 2 g of $Mo(CO)_6$ in 100 mL Decalin) prior to sonication. The sonication was carried out under similar conditions, as described above. Stober's silica[13] has been prepared by base hydrolysis and condensation of tetraethyl orthosilicate (TEOS) in an aqueous ethanol medium containing ammonia. The as-made Stober's silica was heated at 750 °C for 6 h in ambient air to remove the surface bonded water. The resulting amorphous preheated silica is termed "activated-silica," which is free from the population of surface hydroxyl groups.

Characterization. IR spectra were recorded using a Nicolet (impact 410) FT-IR spectrometer, using transparent pellets of the compounds in KBr (Aldrich, FT-IR grade) matrixes. KBr was used as the background file. All spectra were measured from approximately 4000 to 400 cm^{-1}; the number of scans was typically 75, with a resolution of 4 cm^{-1}. Differential scanning calorimetry (DSC) and thermogravimetric analysis (TGA) of the dried blue product was carried out on a Mettler DSC-30 and a Mettler TG-50 (TC11 TA Processor), respectively, with a heating rate of 10 deg/min, under the flow of nitrogen. The X-ray diffraction patterns were recorded by employing a Rigaku X-ray diffractometer (Model-2028, Cu Kα). The UV−visible absorbance spectra of the blue product was obtained using a Varian (model-DMS 100S) UV−visible spectrophotometer. The transmission electron micrographs and selected area diffraction patterns were obtained by employing a JEOL-JEM 100SX electron microscope. Samples for the TEM measurements were obtained by placing a drop of suspension from the as-sonicated slurry on a carbon-coated Formvar copper grid (400 mesh, electron microscopy sciences) followed by air-drying to remove the solvent. X-ray photoelectron spectra (XPS) of the blue product were obtained in an industrial Kratos AXIS-HS system with an Al (Kα) monochromatic source (1486.6 eV). The energy scale was calibrated using the Si line of the scotch tape used to paste the sample powder. ESR spectra were recorded on a Bruker ER 083 CS spectrometer operating at X-band frequency (ν = 9.7 GHz), with 100 kHz magnetic field modulation.

Results and Discussion

A. Blue Oxide. Stabilized pentavalent molybdenum oxide usually has the essential structure of MoO_3, due to the nearness of ionic radii of Mo^{5+} and Mo^{6+}. MoO_3 consists of a bilayer of distorted corner-linked [MoO_6] octahedra running parallel to the [010] direction; each bilayer is held together by weak van der Waals forces, providing easy cleavage along (010) planes.[1b] Molybdenum bronzes, A_xMoO_3 (A = H, alkali, and alkaline metals), have layered type structures, with edge and corner-sharing [MoO_6] octahedra forming infinite two-dimensional sheets that are held together by the A cation. In the case of hydrogen molybdenum bronzes, [MoO_6] octahedra of $(MoO_6)_n$ sheets cause minor rearrangements in the Mo−O framework

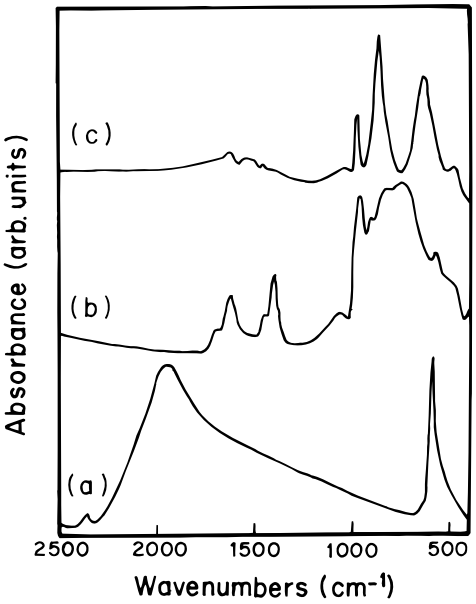

Figure 1. FT-IR spectra of (a) $Mo(CO)_6$, (b) blue oxide, and (c) dehydrated blue oxide.

by the insertion of protons into MoO_3 interlayers. It is naturally accepted that the formation of reduced Mo ions such as Mo^{5+} and/or Mo^{4+} and change in the Mo coordination sphere (octahedra → lower symmetry) are brought about by insertion of the A cation. The formation of oxygen-deficient type pentavalent molybdenum oxide by the reduction of MoO_3 was explained by the crystallographic shear rearrangement. The random vacancy sites stabilize reduced molybdenum valences such as Mo(V) for singly vacant sites. On the other hand, MoO_2 is composed of strings of $[MoO_6]$ octahedra joined by edges along the [100] direction and connected by corner-sharing into a three-dimensional structure.

Infrared Studies. Infrared (IR) spectra of the reactant and product (Figure 1) lend support to our observation of the sonochemical oxidation of $Mo(CO)_6$ to molybdenum oxide under our experimental conditions. A band at 2000 cm^{-1} in the spectrum of reactant, which is diagnostic[14] of the carbonyl stretching vibration, disappears in the product. Also, the product shows IR absorption bands in the region of 600−1000 cm^{-1}, corresponding to the Mo═O and Mo−O vibrational modes. A sharp absorption band around 960 cm^{-1} is characteristic of terminal molybdenum oxygen double-bond (Mo═O) stretching, indicating the presence of a strong molybdenum−oxygen bond of the molybdenyl type. The strong diffuse absorption band between 900 and 600 cm^{-1} corresponds to the overlapping of vibrational bands of Mo−O single bonds and Mo−O−Mo linkages in an octahedral, as well as tetrahedral, symmetry.[15a,b] The Mo ions in the "blue oxides" can exhibit two types of coordination—tetrahedral coordination and more common octahedral coordination—and thus they may have T_d or O_h symmetry with respect to oxygen atoms. In general, the IR spectra of Mo blue oxides are quite complex, owing to the two types of symmetry groups of T_d and O_h.[15b] The presence of water molecules in the initial product yields a broad absorption between 3600 and 3000 cm^{-1} correspond to the OH stretching of hydrogen-bonded H_2O and coordinated H_2O in the IR spectrum (not included in Figure 1). However, a greater wealth of information about the bonding nature of the H_2O can be obtained distinctly in the region of 1300−1700 cm^{-1}. The appearance of two absorption bands at 1640 and 1400 cm^{-1} (bending mode of OH) shows the presence of coordinated, as well as the hydrogen-bonded, H_2O, respectively, in the blue

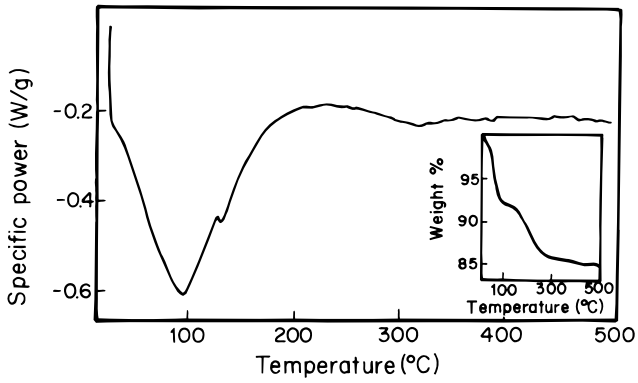

Figure 2. DSC profile of the blue oxide (inset: TG curve of the blue oxide).

oxide,[15c] while the IR spectra of dehydrated oxide (at 300 °C for 8 h) shows the absence of an absorption band between 1300 and 1700 cm^{-1}, corresponding to the bending mode of water molecules. The absorption bands corresponding to the metal oxygen bonds become simple, owing to the O_h symmetry of the resulting oxides (MoO_3 and MoO_2) upon calcination. The sharp absorption band at 960 cm^{-1} corresponds to the terminal Mo═O character that is retained. The other two strong absorption bands at around 880 and 640 cm^{-1} are characteristic of antisymmetric stretching of Mo−O−Mo linkage and the ν_{Mo-O} stretching mode, respectively.

Thermal Analysis. DSC measurements on the blue product were carried out in order to ascertain the nature of the blue product and whether it exists as well-known hydrogen bronzes or as hydrated pentavalent molybdenum oxide. The DSC of the blue product shows two endotherms at around 100 and 150 °C (Figure 2). These two successive endotherms can be attributed to the elimination of hydrogen-bonded water (100 °C), followed by the elimination of coordinated water (150 °C). The highly broadened nature of the first endotherm at 100 °C is probably due to the presence of organic impurities as well. According to Sotani et al.,[16] hydrogen bronzes would yield exotherms (depending on the type of bronze) in the DSC profile at a temperature between 300 and 400 °C, due to the hydrogen elimination. The absence of exothermic response in the temperature region of 300−450 °C in the DSC profile eliminates the possibility of hydrogen bronze formation under sonochemical conditions. A small exothermic hump immediately after the dehydration endotherms in the DSC profile at around 200−250 °C can be assigned to the decomposition of unstable Mo_2O_5 to stable MoO_2 and MoO_3 oxides (confirmed by powder XRD). The thermogravimetric analysis (TG) of the blue powder shows (inset of Figure 2) weight losses in two steps, as expected. The weight losses correspond to the loss of two water molecules, the total weight loss (∼13%) being consistent with the following reaction:

$$Mo_2O_5 \cdot 2H_2O \xrightarrow{100\ ^\circ C} Mo_2O_5 \cdot H_2O \xrightarrow{140\ ^\circ C} Mo_2O_5 \xrightarrow{200-250\ ^\circ C} MoO_3 + MoO_2 \quad (1)$$

Accordingly, the combined results of DSC and TG analysis reveal that the sonication product is $Mo_2O_5 \cdot 2H_2O$. The water molecule in the blue product is presumably taken up from the atmosphere. However, sonication of $Mo(CO)_6$ under dry air/oxygen again yields blue oxide with a lower water content (∼9%), which we did not characterize further. This observation indicates that the water may orginate from two possible sources: (i) the inherent existence of water content in the ambient air, precursor, and solvent, and (ii) the in situ generation

of H_2O under sonochemical conditions. The following possible mechanism will account for the formation of water-stabilized blue oxide.

Mechanism of Sonochemical Process. Most of the chemical reactions, which are brought by ultrasonic waves intense enough to produce cavitation, are oxidation and decomposition.[17] It has been recognized that the absorption of ultrasound by alkanes can lead to the formation of H• radicals and C−C bond cleaved products. Suslick and co-workers[17a] have identified the generation of CO_2 and CO as the sonochemical product of alkanes, apart from the normal cleaved products of alkane and H_2, if O_2 is present. The sonochemical reaction can be understood by considering the reaction sites:[11a] (i) the gas-phase within the collapsing cavity "bubble", where elevated temperatures and high pressures are produced; (ii) the interfacial region or liquid phase immediately surrounding the gas-phase region, where the temperature is lower than in the gas-phase reaction zone, but still high enough for a sonochemical reaction. Generally, all the sonochemical reactions can be explained by a radical mechanism,[17a] where the primary step for the sonochemical reaction is the hydrogen abstraction from the solvent (R) or substrates. Accordingly, the following possible elementary reaction that can occur in the bubble leads to the generation of water molecule has been proposed:

$$R \rightarrow R^* + H^\bullet \quad \text{(sonolysis)} \tag{2}$$

$$O_2 \rightarrow O^\bullet \quad \text{(sonolysis)} \tag{3}$$

$$2H^\bullet + O^\bullet \rightarrow H_2O \tag{4}$$

From the thermal analysis data of the blue oxide, it is possible to calculate the amount of water generated under our experimental conditions semiquantitatively. The total water content in the blue oxide prepared under dry air/oxygen condition was ~9%, estimated using the TGA results. This value is much higher than the inherent water content of the starting materials, which is roughly around 3%. Therefore, the remaining ~6% of water in the blue oxide can be attributed to the in situ generation according to the sonochemical reactions 2−4.

The sonochemical oxidation of molybdenum carbonyl would not occur in the bubble, due to its low vapor pressure. Therefore, the sonochemical reaction of $Mo(CO)_6$ appears to take place in the interfacial region:

$$2Mo(CO)_6 + {}^{17}/_2O_2 \rightarrow Mo_2O_5 + 12CO_2 \quad \text{(sonolysis)} \tag{5}$$

Thus the formed water molecule in the bubble (eq 4) may diffuse into the interfacial region or the water molecules that are available from the atmospheric air, precursor, and solvent stabilize the unusual pentavalent molybdenum oxide:

$$Mo_2O_5 + 2H_2O \rightarrow Mo_2O_5 \cdot 2H_2O \tag{6}$$

The above possible mechanism for the formation of the blue oxide is consistent with explanations in the literature for a sonochemical reaction.

X-ray Diffraction and TEM. The powder X-ray diffraction (XRD) showed (Figure 3a) the absence of diffraction peaks, indicating the crystallographically amorphous nature of the initial blue product. The amorphous nature of the blue product was further confirmed by the selected area electron diffraction (SAED) pattern, and it demonstrates a diffuse ring pattern characteristic of amorphous materials (see inset of Figure 4). Heating the product at 300 °C for 2 days in a flow of N_2 yielded a pale yellow powder, and diffraction peaks were observed,

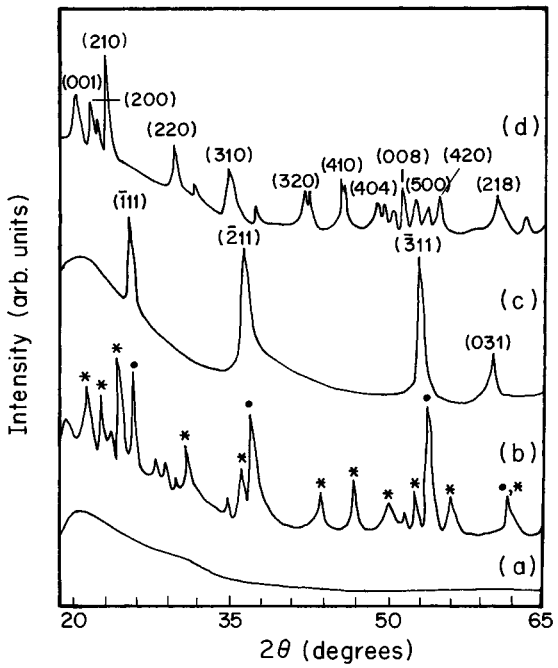

Figure 3. XRD pattern of blue powder: (a) as-made, (b) heated at 300 °C under N_2 (* denotes MoO_3 and ● denotes MoO_2), (c) heated at 300 °C under H_2, (d) heated at 300 °C under O_2.

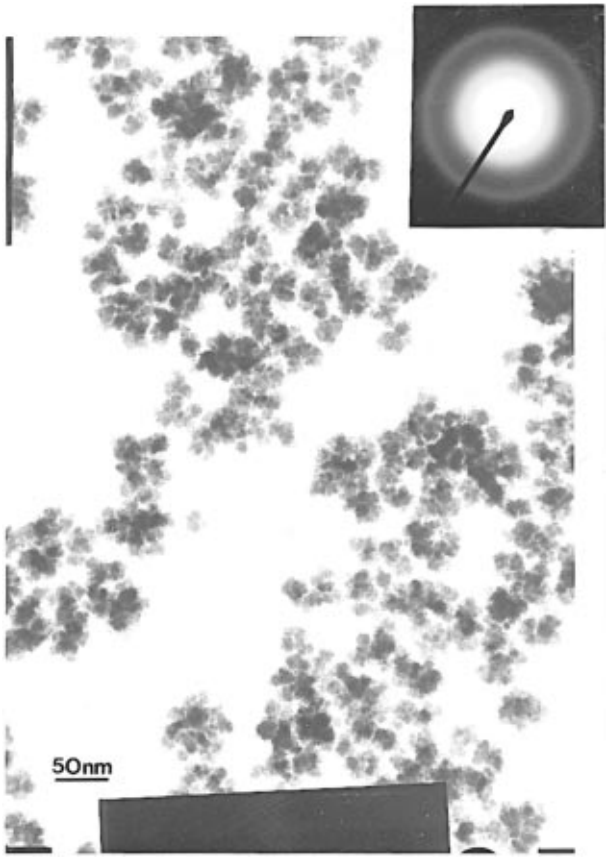

Figure 4. Transmission electron micrograph of blue oxide (inset: associated SAED pattern).

corresponding to a mixture of MoO_3 and MoO_2 phases (Figure 3b) and confirming IR and thermal analysis observations. Heating the blue oxide at 300 °C for 2 days under a hydrogen atmosphere yields a crystalline MoO_2 phase (Figure 3c). On the other hand, heating the initial blue oxide at the same temperature under an oxygen atmosphere yields MoO_3 (Figure

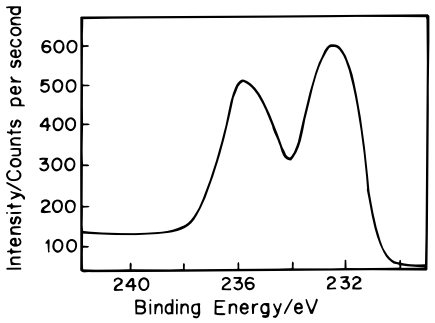

Figure 5. Mo 3d XPS spectrum of blue oxide. Only the Mo (3d) spin−orbit component is shown, for clarity.

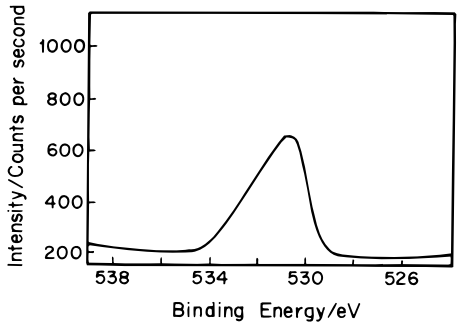

Figure 6. O 1s XPS spectrum of blue oxide.

3d). The diffraction patterns are indexed on the basis of Joint Commission on Powder Diffraction Standards (JCPDS) data.

Transmission electron micrographs (Figure 4) of the blue oxide reveal the nature of the particulates. The powder consists of fairly uniform platelet particles, with an average size of 20 nm. The particles are spongy in nature and are held in a soft-aggregate assembly. The inset of Figure 4 shows the SAED of the initial product, which shows a ring pattern characteristic of amorphous material and confirms the powder XRD result.

XPS Studies. X-ray photoelectron spectroscopy allows for determination of the oxidation state and chemical structure of the amorphous materials. The Mo 3d spectrum of the blue oxide is shown in Figure 5, depicting a broad doublet corresponding to the $3d_{5/2}$ and $3d_{3/2}$ states (spin−orbit coupling of a 3d state). The peak is quite symmetrical. The broad signal, centered at 231.5 eV, is characteristic of pentavalent Mo $3d_{5/2}$ binding energy.[6,7a,18] The separation between the two peaks (spin−orbit components) is 3.4 eV, consistent with the value reported in the literature. The appearance of a single Mo(3d) doublet, representative of a single oxidation state, is associated with blue oxide. Unlike the sharp peaks observed for Mo oxides, we obtained a broadened Mo(V) (fwhm ∼2 eV) 3d component, which has been observed on a conducting substrate. In the literature, the broadness of the Mo 3d peak has been attributed to the effect of charging, amorphicity, chemical interactions, and aggregate size.[19] The observed large fwhm (full width at half-maximum) value of the XPS signal cannot be attributed to broadening due to surface charging, since the substrate is highly conductive (silicon paste). The broadness of the XPS signal may due to the combined effects of the amorphous nature and nanorange particles of the blue oxide. The pentavalent oxidation state of molybdenum in the initial blue oxide was further confirmed by the potentiometric titration, using Ce(IV) as an oxidant, and was determined as 5.02 ± 0.02.

The O 1s XPS spectrum of the initial blue oxide is shown in Figure 6. This again shows a very broad signal at around 530.5 eV. This 530.5 eV O (1s) peak is attributed to the oxygen atom bonded to the pentavalent molybdenum. The peak is quite asymmetric in nature, compared to that of the 3d XPS spectra

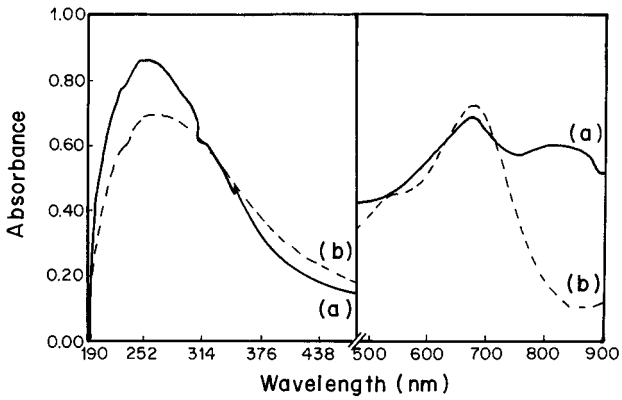

Figure 7. UV−visible spectra of the blue oxide (a) in acetonitrile and (b) in acidic medium.

of Mo. The asymmetry in the O 1s signal can be ascribed to the presence of water molecules in the initial product. The shoulder at around 533.1 eV in the O 1s spectrum is characteristic of O (1s) peaks caused by the water molecule.[20]

UV−visible Spectroscopy. To obtain more information about local structure around the metal ion in the amorphous blue product, UV−visible spectroscopy was applied. The UV−visible spectrum (Figure 7a) of the blue oxide in acetonitrile shows three absorption bands of around 800, 670, and 250 nm. The electronic spectra of the simple hydrated M(V) oxide can, in principle, display d−d transitions in which the single unpaired electron is promoted from the d_{xy} orbital to the doubly degenerate Mo═O (π^*) level or to the two higher d(σ^*) levels.[21] The two observed peaks in the visible region at 800 and 670 nm can be attributed to the d−d transition. In comparison with the spectra of Mo(V) compounds,[21b] the maxima observed at 800 nm band lead to the assignment of a $^2B_2 \rightarrow {}^2B_1$ transition with the other visible band at 670 nm corresponding to a $^2B_2 \rightarrow {}^2E$ transition.

The broad absorption band (220−350 nm) centered at around 250 nm in the UV region is ascribed to the expected ligand−metal charge transfer (LMCT) bands originating from the promotion of electrons from the filled Mo═O (π) levels to the d orbitals. The position of the LMCT absorption band is known to be sensitive to the local symmetry of metal ion.[22] For oxygen ligands, a more energetic transition is expected for a tetrahedral coordinated Mo than for an octahedral one. The [MoO_4] and [MoO_6] LMCT bands normally appear at the 220−270 nm range and 270−340 nm, respectively. Distortion of the symmetry of the [MoO_6]/[MoO_4] structure would cause the LMCT band to shift to a shorter wavelength. The observed broad nature of the LMCT absorption band of the blue oxide (Mo^{5+}) cannot be ascribed to a simple type of geometry (T_d or O_h); however, it can be attributed to the existence of both [MoO_4] tetrahedra (T_d) and [MoO_6] octahedra (O_h) having a distorted symmetry. The observed position of the electronic transition of the blue oxide is consistent with the various solvents. A pronounced shift was observed in the acidic solution of the blue oxide (Figure 7b). The higher energy (UV region) LMCT band of the blue oxide both in acetonitrile and in acidic solution (dilute sulfuric acid) is virtually similar in shape. However, a small shift of 10−15 nm to a longer wavelength on the LMCT band was detected for the blue oxide in acidic medium, probably due to the formation of a protonated isopoly Mo(V) species.[23] The appearance of an absorption band at 520 nm for the oxide in acidic solution has no counterpart in the spectrum of oxide in the acetonitrile. We suggest that this change reflects the generation of more delocalized protonated isopoly Mo(V) species in acidic medium.

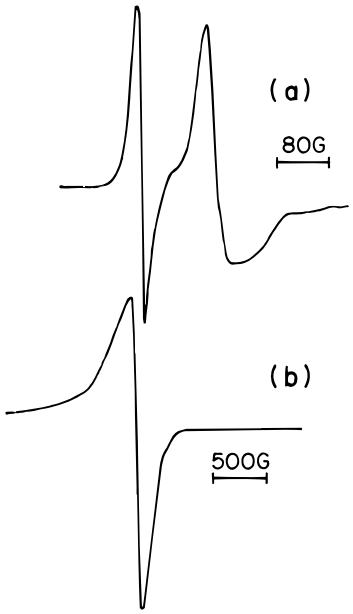

Figure 8. EPR spectra of (a) blue oxide and (b) dehydrated blue oxide.

EPR Studies. The electron paramagnetic resonance (EPR) spectrum of the blue product in the solid-state shows (Figure 8a) a doublet feature with $g = 1.972$. The EPR spectral pattern of the water-stabilized pentavalent molybdenum oxide is different from the expected EPR spectra[24] of Mo^{5+}, a d^1 cation, consisting of a strong singlet from the nonmagnetic nuclei ^{92}Mo, ^{94}Mo, ^{96}Mo, ^{98}Mo, and ^{100}Mo (total natural abundance 74.32%) or a hyperfine "sextet" pattern from magnetic nuclei, ^{95}Mo and ^{97}Mo (total abundance 25.68%). On the basis of spectral comparisons with the literature, the generation of an unusual doublet pattern for the blue oxide is probably due to the superhyperfine coupling of proton ($I = {}^1/_2$) to Mo(V) ($I = 0$). Proton hyperfine splitting in the spectra of our solid blue oxide material arises from the combined effects of the isotropic Fermic contact interaction and the anisotropic (electron-spin:nuclear-spin) dipolar interactions, due to their fixed orientation in the lattice.[25] The observed $g = 1.972$ value is in reasonably good agreement with those g-factors of related Mo(V) compounds.[26] The deviation of a g-factor from the free electron value ($g_e = 2.0023$) basically arises from spin−orbit interaction on the metal atom. The lower g-value of the blue powder indicates the strong spin−orbit coupling of a d^1 cation of less than a half-filled state. The EPR spectrum of the dehydrated sample (Figure 8b) replaces the doublet with a broad singlet signal ($g = 1.997$). This can be traced to the expected decomposed Mo_2O_5 product [MoO_2:Mo(IV), d^2 system]. The broadening is due to spin−lattice relaxation resulting from interaction on the metal center with the thermal vibrations of the lattice. The collapse of the doublet in the dehydrated sample indicates that the hyperfine splitting arises from a single proton of the coordinated water. From the EPR results of the blue oxide, it is clear that the water molecule coordinated to the Mo center and the unpaired electron of the metal atom are highly delocalized and thus display a simple classic example of the superhyperfine coupling.

B. Silica-Supported Blue Oxide. *TEM Studies.* The nature of the sonochemically deposited blue oxide on silica microspheres was examined using TEM. The morphology of the activated-silica prior to the sonication is shown in Figure 9. The particles were spherical in shape, monodispersed, and free from agglomerated. Magnified TEM images of activated silica (Figure 9b) show the clean and smooth surface, without any foreign impurities. The mean diameter in the TEM micrograph was roughly around 250 nm. Figure 10 shows the TEM

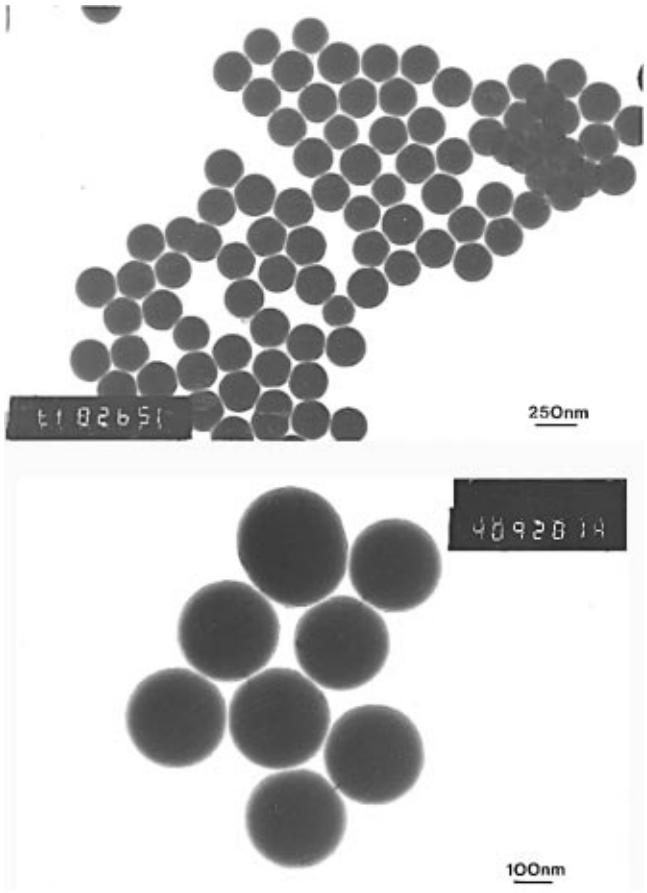

Figure 9. TEM micrograph of Stober's silica: (a, top) bar = 250 nm, (b, bottom) bar = 100 nm.

micrographs of silica coated with blue oxide generated in situ by sonochemical decomposition of $Mo(CO)_6$. Almost all the silica microspheres are totally covered by the blue oxide, without any free silica surface. Each silica particle is well separated and completely covered by blue oxide. A magnified TEM image of silica-core spheres coated with blue oxide on the surface is shown in Figure 10b. It can be seen that the nanoparticles of blue oxide are strongly attached to the surface of silica. It is interesting to see the strongly adhered nature and uniform coating of blue oxide on silica in as-sonicated material (without any further treatment), which is very unique. This observation is notable compared to the sonochemical deposition of amorphous nickel on as-made silica,[27] where we observed that only part of the silica spheres were coated by Ni and that distribution of Ni was not uniform. The lack of adhering nature of nickel on as-made Stober's silica was due to the fact that the screening of the silica surface by the huge amount of silanol groups prevents the accessibility of the Si−O bond for the interaction of Ni. Using IR data, a mechanism of ultrasound-driven dehydrative condensation of hydrogen-bonded silanols to form siloxane links followed by the formation of a bond between nickel and the bridging oxygen of the siloxane links was proposed. On the other hand, strong attachment of elemental Ni to the silica core was observed after heating them at an elevated temperature at which initial nanophasic Ni was converted to polycrystalline form. This can be explained by considering a chemical bonding of nickel to the oxygen of the siloxane link produced by the elimination of silanol links by dehydration at higher temperatures.

IR Investigation. The observed strong attachment of the blue oxide to the activated silica surface in the as-sonicated product may be due to the bonding of Mo to the oxygen of the siloxane

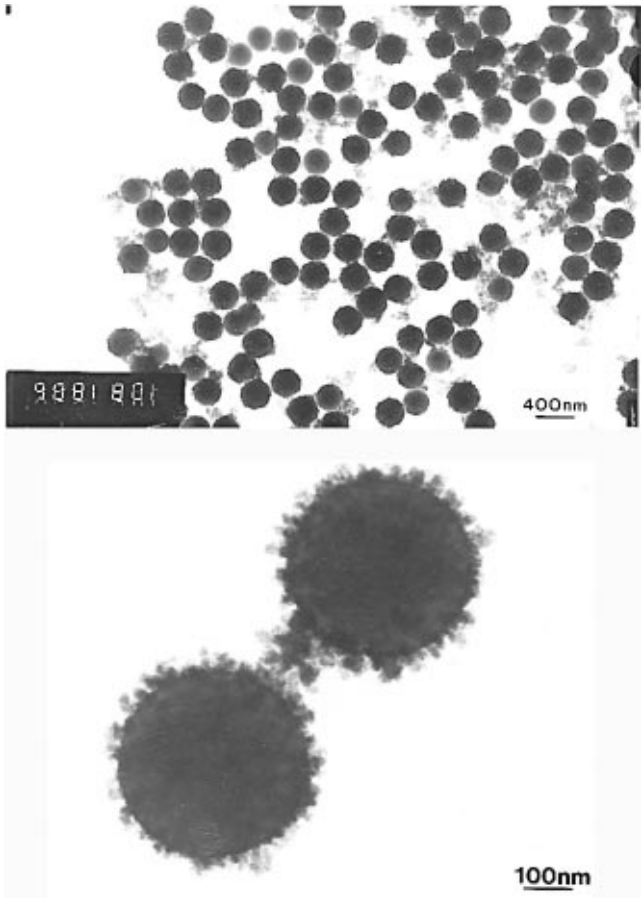

Figure 10. TEM micrograph of silica-supported blue oxide: (a, top) bar = 400 nm, (b, bottom) bar = 100 nm.

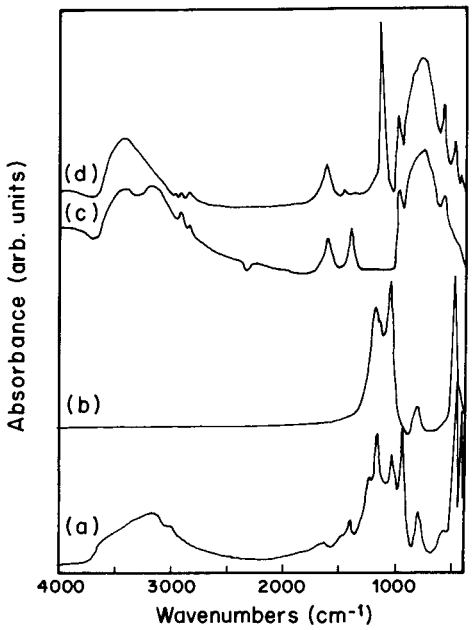

Figure 11. FT-IR spectra of (a) Stober's silica, (b) activated silica, (c) blue oxide, and (d) silica-supported blue oxide.

link (Si−O−Si) upon sonochemical cavitation. This view is strengthened by the our preliminary FT-IR investigations on silica-supported blue oxide and provides a convincing explanation for the strong adhesion of the blue oxide to the silica surfaces. Figure 11 displays the FT-IR spectra of as-made silica, activated-silica, blue oxide, and as-sonicated silica-supported blue oxide.

The assignment of absorption bands of silica can be made by understanding the complex surface structure. Silica is composed of $[SiO_4]$ tetrahedra linked together so that every oxygen atom is common to two tetrahedra. The as-made Stober's silica shows four different absorption bands in the spectral region of 400−4000 cm^{-1}. The surface of the as-made Stober's silica usually contains four types of oxygen species:[28] (a) the oxygen associated with single free silanols, (b) oxygen in the network of hydrogen-bonded silanols, (c) silanol oxygen bonded to the physisorbed water, and (d) the bridging oxygen in the siloxane links (Si−O−Si). The broad band between 3700 and 2700 cm^{-1} corresponds to OH stretching of surface silanols (a, b, c types of bonding). The absorption bands in the region of 1600−400 cm^{-1} can be assigned to the vibrational mode of siloxane links.[29] The observed broad complex band in the wavenumber region of 1200−1000 cm^{-1} corresponds to the asymmetric stretching (AS) vibrational mode of the Si−O−Si bridge of the siloxane link. It is very difficult to separate the different components of the vibrational mode of the siloxane bridge for the amorphous materials. However, existence multiples in the AS mode of amorphous Stober's silica is probably due to the presence of long-range surface disorder in the siloxane links, owing to the surface hydroxyl populations. Symmetric stretching (SS) of the O atom along a line bisecting the axis formed by the two Si atoms characterizes the vibrational mode of the absorption band centered at 810 cm^{-1}. Racking (R) of the O atom of siloxane on an axis through the two Si atoms characterizes the vibrational frequency of the lowest frequency absorption band centered at 460 cm^{-1}. The IR spectrum of the activated-silica shows (Figure 11b) only three absorption band characteristics of the siloxane links. The absence of an absorption band in the OH stretching region suggests the breaking of the silanol bonds upon thermal treatment. The dehydroxylation of silanol groups with thermal treatment produces highly strained Si−O−Si networks.[28] The peak position and shape of R and SS bands are virtually unchanged upon heating. However a greater ordering is noticed in the AS band, which shows a doublet in the wavenumber region of 1200−1000 cm^{-1}. The sharp band at 1060 cm^{-1} corresponds to the characteristic oxygen asymmetric stretch mode (AS1, optically active, in-phase motion of adjacent oxygen atoms). The other AS component at around 1180 cm^{-1} is probably due to the strained siloxane links generated by thermal dehydroxylation of silanols. According to Almeida and coworkers[30] the AS motion actually has a second component, AS2 (apart from the AS1), which is optically inactive and displays out-of-phase motion of adjacent oxygen asymmetric stretching, which normally appears at above 1200 cm^{-1}. Conventional transmission IR measurements should only excite the AS1 (optically active) absorption component.[31] Both the AS1 and AS2 modes can be resolved by using an oblique-incidence (60° from normal), p-polarized infrared absorption. The observed splitting of AS in a conventional IR spectrum is interpreted as due to the disorder-induced coupling between the AS1 mode and the optically weak AS2 mode, due to the presence of strained Si−O−Si networks, which can give rise to the splitting of AS modes as recognized earlier.[30] Gaskell and Johnson[32] have observed the splitting of the AS mode by using conventional transmission IR, in going from crystalline quartz to amorphous SiO_2 (order → disorder transition). Therefore, it is very clear that the splitting of the AS mode of activated SiO_2 is attributed to the existence of long-range surface disorder induced by the strained Si−O−Si links.

For comparison, the IR spectrum of blue oxide is included in Figure 11. It can be seen that the two humps in the OH

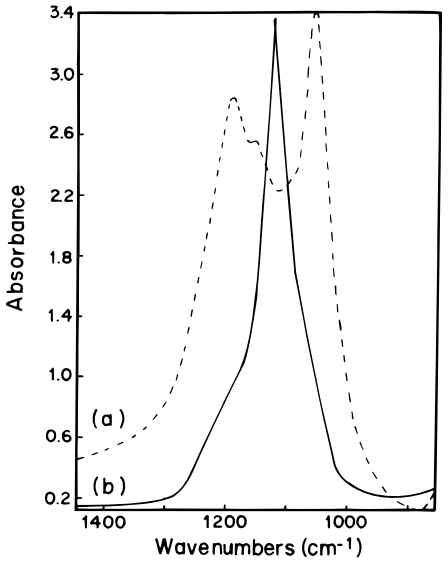

Figure 12. FT-IR Si−O−Si AS band of (a) activated-silica and (b) silica-supported blue oxide.

stretching (3500−3000 cm^{-1}) correspond to hydrogen-bonded and coordinated water (Figure 11c). The IR spectrum of the silica-supported blue oxide shows (Figure 11d) a significant change in the absorption profile of silica, as well as the blue oxide, upon ultrasound irradiation. The product spectrum shows (Figure 11d) the absence of an absorption band, corresponding to the OH bending of hydrogen-bonded H_2O at 1400 cm^{-1}. The absence of hydrogen-bonded water in the silica-supported blue oxide is also reflected in a marked change in the spectral features of the OH stretching (3700−2700 cm^{-1}) region. A pronounced change was noticed in the IR spectral region of the AS mode of the siloxane link (Figure 12). The doublet of the activated silica AS band was replaced by a sharp band near 1110 cm^{-1}, corresponding to the AS1 mode indicating a surface modification of the blue oxide coating by ultrasonic cavitation. A higher frequency shift of 50 cm^{-1} was observed for the AS1 mode upon deposition of blue oxide, probably associated with the bonding change around the [SiO_4] tetrahedra. The Si−O stretching force constant in the SiO_2 depends on both the Si−O−Si bridging angle (π) and the Si−O distance.[30] The force constant will increase slightly with π. The shift of the AS mode (50 wavenumbers) could be due in part to a certain degree of new chemical bonding, i.e., the formation of Si−O−Mo species, which decreases the Si−O length and increases the π. The splitting of the AS mode of SiO_2 disappeared upon sonochemical deposition of the blue oxide on the SiO_2 surface (Figure 12). However, a less intense small shoulder in the region of 1200 cm^{-1} could still be detected, typifying a low degree of disorder splitting due to the depletion of strained siloxane networks of amorphous SiO_2 upon sonochemical deposition of blue oxide. Thus, the decreased intensity of the AS2 mode reveals surface ordering by breaking the strained siloxane networks of the silica upon ultrasound cavitation. The marked change in the nature as well as peak position of the AS mode of the silica indicates ultrasound-induced surface modification of silica (breaking of strained Si−O−Si links), which facilitates the strong bonding of Mo, that is, Si−O−Mo interfacial bonds. Thus ultrasound-induced cavitation appears to play a dual role in oxidative decomposition of molybdenum carbonyl, as well as in activation of the silica surface for the adhesion of the resulting blue oxide. Alternatively, IR could not yield much information in the Mo−O stretching spectral region, due to the overlapping of various different modes of ν_{Mo-O} bands.

One of the beneficial properties of silica is that the surface can be chemically modified by various species, utilizing the strength of the Si−O bond. It has been shown that desirable organic functionalities can be chemically bonded to the silica surface.[33] On the other hand, the interaction between the oxide species or metals and the silica surface is explained by the bonding contributions via chemical interaction between the support and active phase (formation of interfacial bonds).[18,34] Zingg et al.[18] have identified the presence of both tetrahedrally and octahedrally coordinated Mo oxide species in Mo/Al_2O_3 catalyst. They claim that the presence of tetrahedrally coordinated Mo(VI) oxide species reduced to tetrahedrally coordinated Mo(V) oxide species under thermal reduction is responsible for the good adhesion and distribution of the active phase on the support material. Several research groups have studied the interaction between the silica support and surface Mo species.[34] The nature of bonded sites on supported molybdena catalysts has been the subject of controversy in the literature. The bonding of the molybdate species to the silica surface is likely to be covalent in nature. The molybdate species is usually represented as the negatively charged species, MoO_4^{2-}. Similarly, because of the high acidity of silica, the polarity of Si−O bonds in silica is Si−O^-. Because the direction of polarization in both species is the same, bonding results in a complex that is neutral in character, with relatively weak covalent Si−O−Mo bonds.[34a,b] Gamboro and Fierro[34c] indicated that on MoO_3/SiO_2, adsorption occurs on Mo^{5+} (pentavalent) sites. Che et al.[34d] have prepared a dark brown Mo_2Cl_{10} on SiO_2 by reacting $MoCl_5$ with silica hydroxyl groups. Upon exposure to air, this became dark blue, indicative of the hydrolysis and partial oxidation of Mo_2Cl_{10} to the Mo(V) oxide, which is chemically bound to the silica surface. From the EPR and UV−visible studies of Mo−SiO_2 systems, the formation of a strong chemical bond (Si−O−Mo) seemed to result from a high degree of covalency of the molybdenyl Mo(V) oxide species in a tetrahedral symmetry. Che et al.[34d] were able to identify three types of coordination spheres of Mo^{5+} ions. Under similar bonding interactions, the formation of a Si−O−Mo interfacial link leading to a strong surface attachment of the blue oxide to the silica surface can be reasonably assumed. The formation of strong interfacial chemical bonds in silica-supported blue oxide under cavitation could be favored by the following two factors. (i) The Si−O nucleating sites formed by the ultrasonic breakage of strained siloxane link can expected to be more facile in the formation of interfacial bonds. (ii) High degree of covalent character of the molybdenyl Mo(V) oxide species, $(Mo{=}O)^{3+}$, in the blue product leads to a strong interfacial chemical bond.

The FT-IR spectral results indicate that ultrasonic irradiation promotes the surface ordering of silica and the formation of Si−O−Mo interfacial bonds upon sonochemical deposition of blue oxide, which resembles the structural change caused by heat treatment. To elucidate the electronic situation and nature of the interaction, we have started investigations on the UV−visible, EXAFS, and XPS studies on silica-supported blue oxide.

Conclusion

A novel water-stabilized pentavalent molybdenum oxide has been successfully generated by the controlled sonochemical decomposition/oxidation of molybdenum hexacarbonyl under ambient air at near room temperature. FT-IR reveals that the as-sonicated blue product possesses a molybdenyl bond (Mo═O) and Mo−O character. The thermal analysis and IR data, along with the ESR results, confirm that water molecules stabilize the pentavalent molybdenum oxide. Powder X-ray diffraction

patterns show the amorphous nature of the blue product, which on further calcination yields stable crystalline MoO_3 and MoO_2 phases. The pentavalent oxidation state of the molybdenum in the initial blue product was confirmed by XPS and potentiometric titration methods. The XPS peak widths of the initial blue product were influenced by the nanosized particles, as well as by their amorphous nature. The formation of pentavalent molybdenum oxide was further demonstrated using UV−visible spectral properties. The broad LMCT band of the blue oxide in the UV spectral region (220−350 nm) indicates that the Mo^{5+} ion possesses both tetrahedral (T_d) and octahedral (O_h) symmetry. The EPR results shows that the blue oxide exhibits the superhyperfine coupling structure of pentavalent molybdenum to a proton of the coordinated water. The preliminary TEM studies on silica-coated material show strong adhesion and the well-dispersed nature of pentavalent molybdenum oxide on the silica surface, which is one of the prime desirable characteristics of a potential catalyst. FT-IR absorption spectroscopy studies on silica-supported blue oxide demonstrate that the amorphous silicon dioxide undergoes structural reorganization, eliminating the local disordered structure of strained siloxane links replacing them with more ordered facile Si−O bonds, followed by the formation of Si−O−Mo interfacial linkage upon sonochemical deposition of blue oxide. The Si−O sites generated by the breakage of strained Si−O−Si links upon cavitation could serve as a nucleating centers for the formation of strong interfacial bonds. The sonochemically prepared silica-supported blue oxide appears to meet the "design criteria." These materials promise to have superior catalytic activity to that of the conventional material.

Acknowledgment. We thank the Ministry of Science and Arts, Israel, for a Binational India-Israel grant. We thank Prof. Deutsch, Department of Physics, and Prof. Malik, Department of Life Sciences for extending their facilities to us. The authors thank Dr. Shifra Hochberg for editorial assistance.

References and Notes

(1) (a) Henglein, A. *Chem. Rev. (Washington, D.C.)* **1989**, *89*, 1861. (b) Greenblatt, M. *Chem. Rev.* **1988**, *88*, 31.

(2) Carducci, M. D.; Brown, C.; Solomon, E. I.; Enemark, J. H. *J. Am. Chem. Soc.* **1994**, *116*, 11856. Yao, J. N.; Loo, B, H.; Fujshima, A. *Ber. Bunsen-Ges. Phys. Chem.* **1989**, *93*, 13.

(3) Dowerah, D.; Spence, J. T.; Singh, R.; Wedd, A. G.; Wilson, G. L.; Farchione, F.; Enemark, J. H.; Kristofzski, J.; Bruck, M. *J. Am. Chem. Soc.* **1987**, *109*, 5655.

(4) Cotton, F. A.; Wilkinson, G. *Advanced Inorganic Chemistry*, 3rd ed.; Wiley: New York, 1972; pp 944−975.

(5) Canadell, E.; Provost, J.; Guesdon, A.; Borel, M. M.; Laclaire, A. *Chem. Mater*. **1997**, *9*, 68.

(6) Spevack, P. A.; McIntyre, N. S. *J. Phys. Chem*. **1992**, *96*, 9029.

(7) (a) Clayton, C. R.; Lu, Y. C. *Surf. Interface Anal*. **1989**, *14*, 66. (b) Anbanathan, N.; Rao, K. N.; Venkatesan, V. K. *Appl. Surf. Sci*. **1993**, *72*, 189.

(8) Ng, K. Y. S.; Gulari, E. *J. Catal.* **1985**, *92*, 340. Mol, J. C.; Moulijin, J. A. *Adv. Catal*. **1975**, *24*, 131. Zhang, B.; Li, Y.; Lin, Q.; Jin, D. *J. Mol. Catal*. **1988**, *46*, 229. Anpo, M.; Kondo, M.; Kubokawa, Y.; Louis, C.; Che, M. *J. Chem. Soc., Faraday Trans*. **1988**, *84*, 2771.

(9) Gates, B. C. *Chem. Rev. (Washington, D.C.)* **1995**, *95*, 511. Che, M.; Louis, C. *J. Phys. Chem.* **1987**, *91*, 2875.

(10) Reddy, B. M.; Narsimha, K.; Rao, P. K. *Langmuir* **1991**, *7*, 1551. Williams, C. C.; Ekerdt, J. G.; Jehng, J.-M.; Hardcastle, F. D.; Turek, A. M.; Wachs, I. E. *J. Phys. Chem.* **1991**, *95*, 8781.

(11) (a) *Ultrasound: Its Chemical, Physical and Biological Effects*; Suslick, K. S., Ed.; VCH: Weinheim, 1988. (b) Suslick, K. S.; Choe, S. B.; Cichowlas, A. A.; Grinstaff, M. W. *Nature* **1991**, *353*, 414. (c) Koltypin, Yu.; Katabi, G.; Prozorov, R.; Gedanken, A. *J. Non-Cryst. Solids* **1996**, *201*, 159. (d) Hyeon, T.; Fang, M.; Suslick, K. S. *J. Am. Chem. Soc*. **1996**, *118*, 5492. (e) Cao, X.; Koltypin, Yu.; Katabi, G.; Felner, I.; Gedanken, A. *J. Mater. Res*. **1997**, *12*, 405.

(12) Henglein, A.; Guierrez, M. *J. Phys. Chem*. **1990**, *94*, 5169.

(13) Stobers, W.; Fink, A.; Bohn, E. *J. Colloid Interface Sci*. **1968**, *26*, 62.

(14) Nakamoto, K. *Infrared Spectra of Inorganic and Coordination Compounds*; Wiley: New York, 1963.

(15) (a) Li, C.; Xin, Q.; Wang, K.-L.; Guo, X. *Appl. Spectrosc.* **1991**, *45*, 874. (b) Anvar, M.; Hogarth, C. A.; Theocharis, C. R. *J. Mater. Sci.* **1989**, *24*, 2387. (c) Kondo, J. N.; Iizuka, M.; Domen, K.; Wakabayashi, F. *Langmuir* **1997**, *13*, 747.

(16) Sotani, N.; Eda, K.; Kunitomo, M. *J. Chem. Soc., Faraday Trans*. **1990**, *86*, 1583.

(17) (a) Suslick, K. S.; Gawlenowski, J. J.; Schubert, P. F.; Wang, H. H. *J. Phys. Chem*. **1983**, *87*, 2299. (b) Guierrez, M.; Henglein, A.; Dohrmann, J. K. *J. Phys. Chem*. **1987**, *91*, 6687.

(18) Zingg, D. S.; Makovsky, L. E.; Tischer, R. E.; Brown, F. R.; Hercules, D. M. *J. Phys. Chem*. **1980**, *84*, 2898.

(19) Spevack, P. A.; McIntyre, N. S. *J. Phys. Chem*. **1993**, *97*, 11020.

(20) Peng, X. D.; Barteau, M. A. *Surf. Sci.* **1990**, *233*, 283.

(21) Ung, V. A.; Bardwell, D. A.; Fjeffery, J. C.; Maher, J. P.; McCleverty, J. A.; Ward, M. D.; Williamson, A. *Inorg. Chem.* **1996**, *35*, 5290. Manoharan, P. T.; Rogers, M. T. *J. Chem. Phys.* **1968**, *49*, 5510.

(22) Aritani, H.; Tanaka, T.; Funabiki, T.; Yoshida, S.; Eda, K.; Sotani, N.; Kudo, M.; Hasegawa, S. *J. Phys. Chem.* **1996**, *100*, 19495. Weber, R. S. *J. Catal.* **1995**, *151*, 470.

(23) Nelson, W. H.; Tobias, R. S. *Inorg. Chem*. **1963**, *2*, 985. Papaconstantinou, E.; Pope, M. T. *Inorg. Chem.* **1970**, *9*, 667.

(24) Gao, Z.; Schlick, S. *J. Chem. Soc., Faraday Trans.* **1996**, *92*, 4239.

(25) McConnell, H. M.; Heller, C.; Cole, T.; Fessenden, R. W. *J. Am. Chem. Soc.* **1960**, *82*, 766.

(26) Dowerah, D.; Spence, J. T.; Singh, R.; Wedd, A. G.; Wilson, G. L.; Farchione, F.; Enemark, J. H.; Kristofszki, J.; Bruck, M. *J. Am. Chem. Soc.* **1987**, *109*, 5655. Che, M.; Fournier, M.; Launay, J. P. *J. Chem. Phys.* **1979**, *71*, 1954.

(27) Ramesh, S.; Koltypin, Yu.; Prozorov, R.; Gedanken, A. *Chem. Mater*. **1997**, *9*, 546.

(28) Pelmenschikov, A. G.; Morosi, G.; Gamba, A. *J. Phys. Chem.* **1991**, *95*, 10037.

(29) Kirk, C. T. *Phys. Rev. B* **1988**, *38*, 1255.

(30) Almeida, R. M.; Pantano, C. G. *J. Appl. Phys.* **1990**, *68*, 4225 and references therein.

(31) Hu, S. M. *J. Appl. Phys.* **1980**, *51*, 5945.

(32) Gaskell, P. H.; Johnson, D. W. *J. Non-Cryst. Solids* **1976**, *20*, 153. Gaskell, P. H.; Johnson, D. W. *J. Non-Cryst. Solids* **1976**, *20*, 171.

(33) Ketelson, H. A.; Brook, M. A.; Pelton, R. H. *Chem. Mater*. **1995**, *7*, 1376.

(34) (a) Arena, F.; Parmaliana, *J. Phys. Chem.* **1996**, *100*, 19994. (b) Williams, C. C.; Ekerdt, J. G.; Jehng, J.-M.; Hardcastle, F. D.; Turek, A. M.; Wachs, I. E. *J. Phys. Chem*. **1995**, *95*, 8781. (c) Gambaro, L. A.; Fierro, J. L. G. *React. Kinet. Catal. Lett.* **1981**, *18*, *3*, 495. (d) Che, M.; Louis, C.; Tatibouet, J. M. *Polyhedron* **1986**, *5*, 123.